Self-Induced Transparency in Warm and Strongly Interacting Rydberg Gases

Zhengyang Bai,[1,2,*] Charles S. Adams,[3] Guoxiang Huang,[1] and Weibin Li[2,†]

[1]State Key Laboratory of Precision Spectroscopy, East China Normal University, Shanghai 200062, China
[2]School of Physics and Astronomy, and Centre for the Mathematics and Theoretical Physics of Quantum Non-equilibrium Systems, University of Nottingham, Nottingham, NG7 2RD, United Kingdom
[3]Joint Quantum Centre (JQC) DurhamNewcastle, Department of Physics, Durham University, South Road, Durham, DH1 3LE, United Kingdom

(Received 4 May 2020; accepted 1 December 2020; published 31 December 2020)

We study dispersive optical nonlinearities of short pulses propagating in high number density, warm atomic vapors where the laser resonantly excites atoms to Rydberg P states via a single-photon transition. Three different regimes of the light-atom interaction, dominated by either Doppler broadening, Rydberg atom interactions, or decay due to thermal collisions between ground state and Rydberg atoms, are found. We show that using fast Rabi flopping and strong Rydberg atom interactions, both in the order of gigahertz, can overcome the Doppler effect as well as collisional decay, leading to a sizable dispersive optical nonlinearity on nanosecond timescales. In this regime, self-induced transparency (SIT) emerges when areas of the nanosecond pulse are determined primarily by the Rydberg atom interaction, rather than the area theorem of interaction-free SIT. We identify, both numerically and analytically, the condition to realize Rydberg SIT. Our study contributes to efforts in achieving quantum information processing using glass cell technologies.

DOI: 10.1103/PhysRevLett.125.263605

Introduction.—Strong and long-range interactions between atoms excited in high-lying Rydberg states [1–3] can be mapped onto weak light fields via electromagnetically induced transparency (EIT) [4–10], permitting interaction-mediate optical nonlinearities [11–17] and optical quantum information processing [18–27]. In the EIT approach, ultracold temperatures ($\sim\mu$K) are of critical importance to maintain the dispersive nonlinearity (typically submegahertz). As Doppler broadening ($\propto\sqrt{T}$ with T the temperature) increases from about 100 kHz at 1 μK to gigahertz at 300 K, large thermal fluctuations at high temperatures can easily smear out the nonlinearity [28–31]. To overcome this limitation, recent experiments employ short (nanoseconds) and strong (gigahertz Rabi frequencies) lasers to excite high-density, room temperature (or hot) Rydberg gases [29,30,32] confined in glass cells [33–36]. Through a four-wave mixing process, strong dispersive nonlinearities even exceed the laser strength and thermal effect to realize a single-photon source in the glass cell setting [32]. Though the rapid development in experiments [29,30,32], a theoretical investigation of Rydberg optical nonlinearities that take place on the nanosecond timescale and in room temperature gases is unavailable.

In this work we theoretically investigate dispersive optical nonlinearities of nanosecond light pulses generated in thermal gases of Rydberg atoms excited via a single-photon transition. A crucial requirement to generate significant Rydberg interactions at high temperatures is the high number density of the gas, where inelastic collisions between ground state atoms and Rydberg electrons are strong. We identify a dispersive nonlinear regime of nanosecond pulses where the Rydberg interaction is in the order of gigahertz and surpasses the thermal and collisional effects. Importantly, this Rydberg nonlinearity depends nonperturbatively on the transient dynamics of the atoms. A key finding is that the pulse shapes into a bright soliton, leading to Rydberg self-induced transparency (SIT), in low and high temperature gases. Through numerical and mean-field (MF) calculations, we reveal explicitly the dependence of Rydberg SIT on the Rydberg interaction. This is fundamentally different from conventional (i.e., no two-body interactions) SIT which is governed by the area theorem barely due to light intensities [37]. Our study opens opportunities to implement optical quantum information processing with warm Rydberg gases. As the strong quantum nonlinearity is realized with nanosecond pulses, photon coincidences rates can increase from megabit to gigabit. Such orders of magnitude increasing means Rydberg SIT in room temperature gases could be a much more robust and scalable platform for carrying out optical quantum information processing.

Light-atom interaction.—We consider nanosecond laser pulses (wave vector $\mathbf{k}$ along the z axis) propagating in a high-density gas (density $\mathcal{N}$), as depicted in Figs. 1(a) and 1(b). The laser resonantly couples ground state $|1\rangle$ to Rydberg nP state $|2\rangle$ (with n the principal quantum number) via a single-photon transition [see Fig. 1(c)].

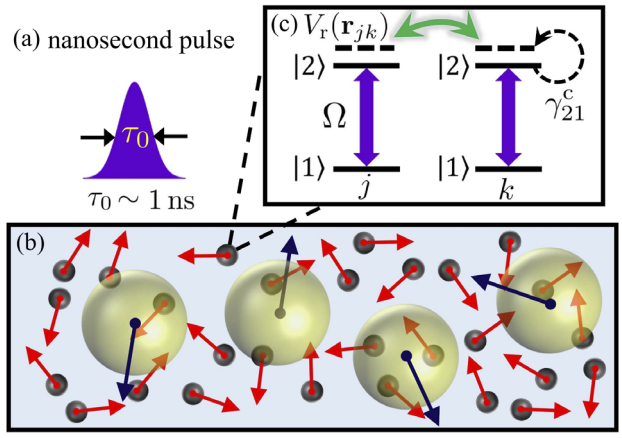

FIG. 1. Light-atom interactions in thermal gases. (a) Nanosecond laser pulses excite atoms from the ground state to Rydberg states. (b) In a gas of warm atoms, the excitation is affected by thermal motions, Rydberg atom interactions, and inelastic collisions between ground state (black dots) and Rydberg (yellow balls) atoms. The latter two depend on the density of the atoms. (c) Level scheme. The laser (Rabi frequency Ω) resonantly couples ground state $|1\rangle$ and Rydberg state $|2\rangle$. The latter experiences strong, long-range van der Waals interactions $V_r(\mathbf{r}_{jk})$ and collisional decay (rate γ_{21}^c). See text for details.

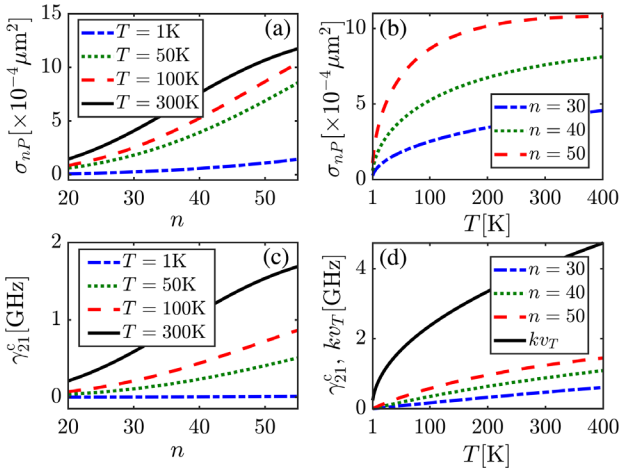

FIG. 2. Collisional cross section and decay rate in Rydberg nP states. The cross section increases with higher n (a) and temperature (b). Collisional decay rates monotonically increase with n (c) and temperature (d). At room temperature, the rate is a few gigahertz for high Rydberg states that is comparable to the Doppler broadening (kv_T). Here the atomic density is $\mathcal{N} = 5 \times 10^{15}$ cm^{-3}, and s-wave scattering length of Cs atoms $a_s \approx 21.7 a_B$ (a_B the Bohr radius).

Two Rydberg atoms (located at $\mathbf{r}_j$ and $\mathbf{r}_k$) interact via the van der Waals (vdW) interaction $V_r(\mathbf{r}_{jk}) = -C_6/|\mathbf{r}_{jk}|^6$ with $\mathbf{r}_{jk} = \mathbf{r}_j - \mathbf{r}_k$ and $C_6 \propto n^{11}$ to be the dispersion coefficient. In this setting, Rydberg electrons frequently collide with surrounding ground state atoms through the polarization interaction. Using the Fermi pseudopotential and neglecting higher partial waves [38], such interaction is approximated to be $V_p(\mathbf{r}_{jk}) \approx 2\pi a_s \delta(\mathbf{r}_{jk})$ [39], where a_s is the s-wave scattering length of the electron-atom collision [40]. This yields the N-atom Hamiltonian ($\hbar \equiv 1$),

$$\hat{H} = \sum_{j=1}^{N} H_j + \sum_{k\neq j}^{N} \left[\frac{V_r(\mathbf{r}_{jk})}{2} \hat{\sigma}_{22}^j \hat{\sigma}_{22}^k + V_p(\mathbf{r}_{jk}) \hat{\sigma}_{22}^j \hat{\sigma}_{11}^k \right],$$

where $\hat{H}_j = \Omega(\mathbf{r}_j)\hat{\sigma}_{21}^j/2 + \text{H.c.}$ is the jth atom Hamiltonian with $\hat{\sigma}_{\alpha\beta}^j = |\alpha^j\rangle\langle\beta^j|$ (α, $\beta = 1$, 2). Here Rabi frequency $\Omega(\mathbf{r}_j) = d_{21}\mathcal{E}(\mathbf{r}_j)$ depends on the slowly varying electric field $\mathcal{E}(\mathbf{r})$ and dipole moment d_{21} between the Rydberg and ground state. To be concrete, Cs atoms will be considered in this work as the respective dipole moment is relatively large compared to other alkali atoms [see Supplemental Material (SM) [41] for details]. Single-photon Rydberg excitation of ultracold Cs atoms has been demonstrated experimentally with nanosecond [42] and continuous lasers [49–52].

In addition to vdW and dipole-dipole interactions between Rydberg atoms, the attractive polarization interaction between electrons and ground state atoms has been extensively studied previously [38,39]. In ultracold gases, it leads to the formation of ultralong-range Rydberg molecules [53–56] and Rydberg polarons [57]. At high temperatures, it causes a spectra shift and inelastic collision due to mixing with other Rydberg states [39]. After compensating the shift with laser detuning, the inelastic collision is characterized by decay rate $\gamma_{21}^c = \mathcal{N} v_T \sigma_{nP}$ [39], where $v_T = \sqrt{2k_B T/M}$ is the thermal velocity (M is the mass of Cs atoms) and σ_{nP} is the collisional cross section [41]. As shown in Figs. 2(a) and 2(b), the cross section becomes larger with increasing n and temperature T. The decay rate moreover depends on atomic densities linearly. In high-density ($> 10^{15}$ cm^{-3}) gases, the decay, e.g., $\gamma_{21}^c \sim 1$ GHz at $T = 300$ K, is comparable to the Doppler broadening [Figs. 2(c) and 2(d)].

Taking into account the inelastic collision, dynamics of the system is described by a set of coupled Maxwell-Bloch equations [43]. In the following, we will focus on propagation of short pulses along the z direction while neglecting the diffraction as the medium is short. Applying the continuous density approximation, this yields the one-dimensional (1D) Maxwell-Bloch equations,

$$i\frac{\partial}{\partial t} w(z) + \Omega(z)\rho_{12}(z) - \Omega^*(z)\rho_{21}(z) = 0, \tag{1a}$$

$$\left[i\frac{\partial}{\partial t} + i\gamma_{21}^c - kv \right] \rho_{21}(z) + \frac{\Omega(z)}{2} w(z) - i\gamma_{21}^c f(v) R_{21}(z) - \mathcal{N}^{1/3} \int dz' dv' f(v') V_r(z'-z) \rho_{22,21}(z', z) = 0, \tag{1b}$$

$$i\left(\frac{\partial}{\partial z}+\frac{1}{c}\frac{\partial}{\partial t}\right)\Omega(z)+\frac{k}{2}\chi(z)\Omega(z)=0, \tag{1c}$$

where $\rho_{\alpha\beta}(z)=\langle\hat{\sigma}_{\alpha\beta}(z)\rangle$ is the mean value of operator $\hat{\sigma}_{\alpha\beta}(z)$, and $w(z)=1$–$2\rho_{22}(z)$ is the population inversion. $R_{21}(z)=\int dv\rho_{21}(z)$ and $\chi(z)=2\mathcal{N}(d_{12})^2\int dv f(v)\rho_{21}(z)/[\varepsilon_0\Omega(z)]$ are the integrated density and susceptibility [43], respectively. $f(v)=1/(\sqrt{\pi}v_T)\exp[-(v/v_T)^2]$ is the 1D Maxwell-Boltzmann velocity distribution. These equations couple to two-body correlation $\rho_{\alpha\beta,\mu\nu}(z',z)\equiv\langle\hat{\sigma}_{\alpha\beta}(z')\hat{\sigma}_{\mu\nu}(z)\rangle$, whose equation is cumbersome and given in SM [41]. Note that spontaneous decay due to finite Rydberg lifetimes (10–100 μs) can be neglected in the dynamics due to mismatch of the timescales [41].

Transmission of light pulses.—We first study optical losses due to the collisional and Doppler effects. The former leads to dissipation directly while the latter causes population partially trapped in Rydberg states, hence reducing the output intensity of the pulse after propagating in the medium (length L). To be concrete, we assume the pulse has a profile $\Omega(z=0)=\Omega_s\mathrm{sech}[(t-t_0)/\tau]$, with Ω_s, t_0, and τ to be the amplitude, center, and duration at the boundary $z=0$. We emphasize that results in the following sections can be equally obtained by considering Gaussian pulses [41].

Using the spatial-temporal solution we evaluate transmission $\eta=\int_{-\infty}^{+\infty}dt|\Omega(L)|^2/\int_{-\infty}^{+\infty}dt|\Omega(0)|^2$ at the output $z=L$. For nanosecond pulses ($\tau\sim 1$ ns), we find that transmission $\eta\sim 1$, indicating that the medium is almost transparent [Fig. 3(a)]. An important feature is that transmission of nanosecond pulses is thermally robust. As shown in Fig. 3(b), the reduction of η is marginal when the temperature increases from 1 to 400 K, though both the decay rate and Doppler broadening are a few gigahertz at 400 K [see Figs. 2(c) and 2(d)].

For long pulses, transmission becomes smaller at higher temperatures [Fig. 3(b)]. When $\tau\gg 10$ ns, η depends on the temperature nontrivially. For example, η decreases and then increases with increasing temperature for $\tau=100$ ns, due to the interplay between the Doppler and collisional effect. We can understand this dependence qualitatively by examining static susceptibility $\tilde{\chi}(T)$ of infinitely long pulses, which is given analytically in SM [41]. By analyzing the imaginary part of $\tilde{\chi}$ [Fig. 3(c)], we find that the collisional decay (Doppler effect) plays a leading role at low (high) temperatures. Moreover the real part of $\tilde{\chi}$ is large at lower temperatures [Fig. 3(d)]. This means that the pulse can gain an optical phase during propagation.

Rydberg SIT of nanosecond pulses.—In the following, we will focus on the high transmission situations, where so-called self-induced transparency [37,59] can form. Without atom-atom interactions, SIT occurs if areas of the input pulse $\theta(z)=\int_{-\infty}^{\infty}\Omega(z)dt=\Omega_s\tau\pi$ are multiples of 2π, i.e., $\Omega_s\tau$ is an even number, governed by the area theorem [59].

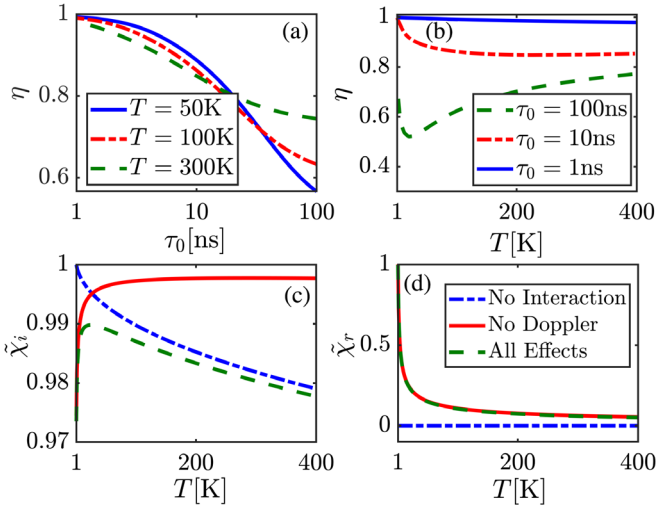

FIG. 3. Transmission of the pulses. The pulse duration (a) and temperature (b) of the medium affect the transmission. When $\tau\sim 1$ ns, $\eta\sim 1$ almost independent of the temperature. Notable absorption is found when $\tau\gg 1$ ns in (a). Transmission varies with temperature nonmonotonically for very long pulses, e.g., $\tau=100$ ns in (b). The imaginary $\tilde{\chi}_i=\mathrm{Im}[\tilde{\chi}(T)]/\mathrm{Im}[\tilde{\chi}_s]$ (c) and real part $\tilde{\chi}_r=\mathrm{Re}[\tilde{\chi}(T)]/\mathrm{Re}[\tilde{\chi}_s]$ (d) of static susceptibility $\tilde{\chi}(T)$ at temperature T, scaled with respect to $\tilde{\chi}_s=\tilde{\chi}(T=1\mathrm{K})$. The maximal $\tilde{\chi}_i$ and maximal absorption for $\tau=100$ ns in (b) both locate around $T=10$ K. The absorption is suppressed at low and high temperatures, due to less Rydberg excitations (hence, decay) caused by the Rydberg blockade and Doppler effect [58], respectively. The Rydberg interaction gives large real part $\tilde{\chi}_r$, especially at low temperatures. The legend in (c) and (d) is the same. We consider Rydberg state $|30P\rangle$ with lifetime 27.79 μs, $L=400$ μm, and $\mathcal{N}=5\times 10^{15}$ cm^{-3}.

This nonlinear effect is rooted solely from high light intensities, which reshape the pulse into a stable, bright soliton, i.e., no absorption or distortion. The nonlinearity reduces the group velocity $[v_g\approx 2\varepsilon_0|\Omega|^2/(k\mathcal{N}d_{12}^2)]$ but does not affect optical phases [59].

Because of the strong Rydberg interaction for $n=30$, the pulse profile is distorted when the input area $\theta(0)=2\pi$ [Fig. 4(a)]. However, its shape is preserved if $\theta(0)=0.35\pi$ [Fig. 4(b)], giving rise to Rydberg SIT. Similar to SIT, the formation of Rydberg SIT can be understood by analyzing the atomic dynamics [37,59]. The dynamics is independent of z since the nanosecond pulse translates in the medium. Crucially important for Rydberg SIT is that coherence $\mathrm{Im}(\rho_{21})$ is symmetric with respect to t_0, i.e., positive (negative) when $t<t_0$ ($t>t_0$) [Fig. 4(c)]. As ρ_{22}, $\rho_{21}\to 0$ when $t\to+\infty$, the light is thus absorbed and then emitted coherently. When T increases from 1 μK to 300 K [Fig. 4(c)], modifications of the dynamics are marginal. Such transient dynamics guarantees the formation of Rydberg SIT at the optimal area $\theta(0)=0.35\pi$.

We define fidelity $F=|\int_{-\infty}^{+\infty}dt\Omega(L)\Omega(0)|^2/\int_{-\infty}^{+\infty}dt|\Omega(L)|^2\int_{-\infty}^{+\infty}dt|\Omega(0)|^2$ to quantify the deformation of the pulses. $F=1$ if the input and output pulse are

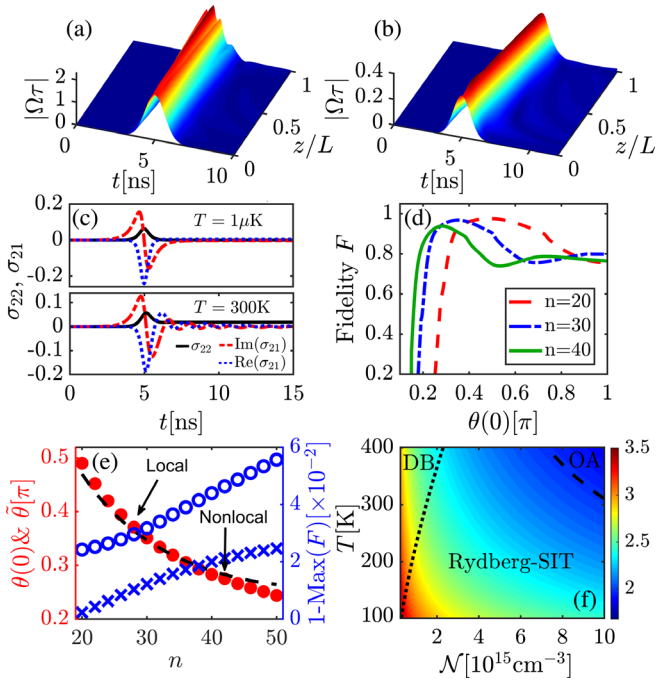

FIG. 4. Rydberg SIT and the optimal area. The pulse is distorted when $\theta(0) = 2\pi$ (a) and stable when $\theta(0) = 0.35\pi$ (b), corresponding to Rydberg SIT. (c) The transient dynamics of atoms at $T = 1$ μK (upper panel) and 300 K (lower panel). $\mathrm{Im}(\rho_{21})$ is symmetric with respect to t_0. The time average of $\mathrm{Im}(\rho_{21})$ is negligibly small at 300 K, which is important to the formation of Rydberg SIT. (d) Fidelity F as a function of initial area $\theta(0)$. Maximal fidelities appear at Rydberg-state-dependent optimal areas. (e) Optimal area (filled circle) and corresponding fidelity at 1 μK (star) and 300 K (empty circle). The MF (dashed line) and numerical calculation agree well. (f) Three regimes of nanosecond pulses, dominated by either the Doppler broadening (DB), Rydberg interactions, or optical absorption (OA). Rydberg SIT forms in the Rydberg interaction dominant region. The color bar shows the ratio of the sum of the Rydberg interaction and Doppler broadening over the collisional decay rate. In panels (a)–(c) and (f), $n = 30$. In panels (d) and (e), the pulse area is varied by changing Ω_s. Other parameters are $t_0 = 5$ ns, $\tau = 1$ ns, $L = 400$ μm, and $T = 300$ K.

identical. When $0 < \theta(0) \leq 2\pi$, F indeed displays a single maximal at $\theta(0) = 0.35\pi$ (see SM [41] for more details). As shown in Fig. 4(d), the optimal area varies when changing n. To systematically understand the dependence of the optimal area on n, we carry out large scale calculations for $20 \leq n \leq 50$. It is found that the optimal area decreases monotonically with increasing n, while the corresponding fidelity is high [Fig. 4(e)]. Note that Rydberg SIT can also be achieved with Gaussian pulses, which lead to similar optimal areas and fidelities as shown in SM [41].

State-dependent optimal areas.—Inspired by the transient dynamics of Rydberg SIT [Fig. 4(d)], we will develop a mean-field theory for the Bloch equation to understand the optimal area. To deal with the two-body interaction term in Eq. (1b), we apply a local field approximation to the two-body correlations, i.e., $\rho_{22,21}(z', z) \approx \rho_{22}(z)\rho_{21}(z)$ [8] as the pulse is much longer than ranges of the Rydberg interaction. With this approximation Eq. (1b) becomes

$$\frac{\partial \rho_{21}}{\partial t} \approx -\gamma_{21}^{c}[\rho_{21} - f(v)R_{21}] - i(kv + u\rho_{22})\rho_{21} - \frac{i\Omega w}{2}, \quad (2)$$

while other equations are not affected formally. Here $u = 2\mathcal{N}^{1/3}\int_0^\infty dz V(z)$ is an effective Rydberg interaction. To avoid divergence in the integral, the vdW potential is modified at short distances to have a soft-core shape, $V(z) \approx C_6/(z^6 + z_m^6)$, when atomic distances are smaller than the blockade radius $z_m = (|C_6|/\Omega_s)^{1/6}$ [2]. This allows us to analytically evaluate the effective interaction $u = 4\pi\mathcal{N}^{1/3}C_6^{1/6}\Omega_s^{5/6}/3$, which depends on the density, Rabi frequency, and Rydberg state.

Depending on the ratio $(kv_T + u)/\gamma_{21}^{c}$, three different regimes of the coherence are obtained approximately according to Eq. (2). Fixing T, a Doppler broadening dominant region appears at low densities when $kv_T > u \gg \gamma_{21}^{c}$, as shown in Fig. 4(f). For sufficiently high densities [dotted line in Fig. 4(f) with $10kv_T = u$] Rydberg interactions overtake the other two effects, i.e., $u > kv_T \gg \gamma_{21}^{c}$. This is the most interesting region where Rydberg SIT can form. Further increasing densities (dashed line, $kv_T + u = 100\gamma_{21}^{c}$), the collisional decay starts to kick in and causes losses. The overall decay will also depend on the propagation distance.

In the following, we will find the optimal areas analytically in the Rydberg interaction dominant region (by neglecting terms involving kv_T and γ_{21}^{c}). As the nonlinear Eq. (2) is difficult to integrate even with this approximation, we will apply the following ansatz solution $\rho_{22} = A[1 - \cos\int_{-\infty}^{t}\Omega_0 dt']$ and $\rho_{21} = -(iB/2)\cos\int_{-\infty}^{t}\Omega_0 dt' + C\rho_{22}$, where A, B, and C are trial parameters, and $\Omega_0 = \sqrt{2\pi}\exp(-t^2/2\tau^2)/\tau$. Such ansatz ensures the symmetry of the transient dynamics, i.e., $\mathrm{Im}[\rho_{21}]$ is symmetric with respect to the pulse center, and $\rho_{12} = \rho_{22} = 0$ when $t \to \infty$. We then approximate the pulse Ω in the MF equation with a Gaussian $\Omega = \tilde{\theta}\exp(-t^2/2\tau^2)/\sqrt{2\pi}\tau$, where $\tilde{\theta}$ is the optimal area to be determined.

Substituting the ansatz to the MF equation, the trial parameters and area $\tilde{\theta}$ can be calculated analytically (see SM [41]). Explicitly, the Rydberg-state-dependent area is given by

$$\tilde{\theta} = \frac{2\pi}{u\tau}(\sqrt{2\pi u^2\tau^2 + \pi^2} - \pi)^{1/2}, \quad (3)$$

which is the key result of the MF calculation. Equation (3) shows $\tilde{\theta} \to 2\pi$ when $u \to 0$, recovering the area theorem in noninteracting SIT [59]. Increasing u, $\tilde{\theta}$ decreases gradually. When compared with numerical data, an excellent agreement is found if $n < 40$. Small deviations for $n > 40$

come from the two-body correlation and collisional decay, which become important gradually with increasing n.

Conclusion and discussion.—In this work, we have studied propagation dynamics of nanosecond pulses in thermal, high-density Rydberg gases. We have shown that strong dispersive optical nonlinearities can be achieved from low to high temperatures. Rydberg SIT can form in thermal atomic gases which is largely immune to the Doppler broadening and collisional decay. A key finding is that the optimal area of Rydberg SIT is reduced by the Rydberg atom interaction. The optimal area and its dependence on the interaction are determined both numerically and analytically.

This work opens exciting opportunities to study nonlinear optics and to implement quantum information processing at nanosecond timescales with warm Rydberg gases. Beyond the present level scheme, one can also achieve strong Rydberg nonlinearities of nanosecond laser pulses via multiphoton excitations (e.g., electromagnetically induced transparency). Benefited from tunable light-atom couplings and spatial excitation selectivity [60], this allows us to study, for example, simultons [61], in strongly interacting Rydberg gases. The strong Rydberg nonlinearity permits us to realize quantum information applications, such as fast optical phase gates [62–65], with Rydberg SIT (see SM [41] for a demonstration).

We are thankful for insightful discussions with Thomas Gallagher, Igor Lesanovsky, Sebastian Slama, Lin Li, Jing Zhang, Jianming Zhao, Junmin Wang. and Stephen Hogan. Z. B. and G. H. acknowledge National Science Foundation (NSF) (11904104, 11975098, 11174080, 11847221), The Shanghai Sailing Program (18YF1407100), China Postdoctoral Science Foundation (2017M620140), and the International Postdoctoral Exchange Fellowship Program (20180040). C. S. A. acknowledges financial support from EPSRC Grant Ref. No. EP/R002061/1, No. EP/M014398/1, No. EP/S015973/1, No. EP/R035482/1, and No. EP/P012000/1, the EU Research and Innovation (RIA) project "RYSQ" project, EU-H2020-FETPROACT-2014 184 Grant No. 640378 (RYSQ) and DSTL. W. L. acknowledges support from the EPSRC through Grant No. EP/R04340X/1 via the QuantERA project ERyQSenS, the Royal Society Grant No. IEC\NSFC\181078, and the UKIERI-UGC Thematic Partnership (IND/CONT/G/16-17/73).

*zhybai@lps.ecnu.edu.cn
†weibin.li@nottingham.ac.uk

[1] D. Jaksch, J. I. Cirac, P. Zoller, S. L. Rolston, R. Côté, and M. D. Lukin, Phys. Rev. Lett. **85**, 2208 (2000).
[2] M. D. Lukin, M. Fleischhauer, R. Côté, L. M. Duan, D. Jaksch, J. I. Cirac, and P. Zoller, Phys. Rev. Lett. **87**, 037901 (2001).
[3] M. Saffman, T. G. Walker, and K. Mølmer, Rev. Mod. Phys. **82**, 2313 (2010).
[4] J. D. Pritchard, D. Maxwell, A. Gauguet, K. J. Weatherill, M. P. A. Jones, and C. S. Adams, Phys. Rev. Lett. **105**, 193603 (2010).
[5] D. Petrosyan, J. Otterbach, and M. Fleischhauer, Phys. Rev. Lett. **107**, 213601 (2011).
[6] W. Li, D. Viscor, S. Hofferberth, and I. Lesanovsky, Phys. Rev. Lett. **112**, 243601 (2014).
[7] O. Firstenberg, C. S. Adams, and S. Hofferberth, J. Phys. B **49**, 152003 (2016).
[8] S. Sevinçli, N. Henkel, C. Ates, and T. Pohl, Phys. Rev. Lett. **107**, 153001 (2011).
[9] Z. Bai and G. Huang, Opt. Express **24**, 4442 (2016).
[10] Z. Bai, W. Li, and G. Huang, Optica **6**, 309 (2019).
[11] A. V. Gorshkov, J. Otterbach, M. Fleischhauer, T. Pohl, and M. D. Lukin, Phys. Rev. Lett. **107**, 133602 (2011).
[12] T. Peyronel, O. Firstenberg, Q.-Y. Liang, S. Hofferberth, A. V. Gorshkov, T. Pohl, M. D. Lukin, and V. Vuleti, Nature (London) **488**, 57 (2012).
[13] A. V. Gorshkov, R. Nath, and T. Pohl, Phys. Rev. Lett. **110**, 153601 (2013).
[14] O. Firstenberg, T. Peyronel, Q.-Y. Liang, A. V. Gorshkov, M. D. Lukin, and V. Vuleti, Nature (London) **502**, 71 (2013).
[15] B. He, A. V. Sharypov, J. Sheng, C. Simon, and M. Xiao, Phys. Rev. Lett. **112**, 133606 (2014).
[16] H. Busche, P. Huillery, S. W. Ball, T. Ilieva, M. P. A. Jones, and C. S. Adams, Nat. Phys. **13**, 655 (2017).
[17] Q.-Y. Liang, A. V. Venkatramani, S. H. Cantu, T. L. Nicholson, M. J. Gullans, A. V. Gorshkov, J. D. Thompson, C. Chin, M. D. Lukin, and V. Vuleti, Science **359**, 783 (2018).
[18] D. Maxwell, D. J. Szwer, D. Paredes-Barato, H. Busche, J. D. Pritchard, A. Gauguet, K. J. Weatherill, M. P. A. Jones, and C. S. Adams, Phys. Rev. Lett. **110**, 103001 (2013).
[19] L. Li and A. Kuzmich, Nat. Commun. **7**, 13618 (2016).
[20] D. Tiarks, S. Schmidt, G. Rempe, and S. Dürr, Sci. Adv. **2**, e1600036 (2016).
[21] D. Tiarks, S. Schmidt-Eberle, T. Stolz, G. Rempe, and S. Dürr, Nat. Phys. **15**, 124 (2019).
[22] H. Gorniaczyk, C. Tresp, J. Schmidt, H. Fedder, and S. Hofferberth, Phys. Rev. Lett. **113**, 053601 (2014).
[23] S. Baur, D. Tiarks, G. Rempe, and S. Dürr, Phys. Rev. Lett. **112**, 073901 (2014).
[24] W. Li and I. Lesanovsky, Phys. Rev. A **92**, 043828 (2015).
[25] D. Tiarks, S. Baur, K. Schneider, S. Dürr, and G. Rempe, Phys. Rev. Lett. **113**, 053602 (2014).
[26] H. Gorniaczyk, C. Tresp, P. Bienias, A. Paris-Mandoki, W. Li, I. Mirgorodskiy, H. P. Bchler, I. Lesanovsky, and S. Hofferberth, Nat. Commun. **7**, 12480 (2016).
[27] C. R. Murray and T. Pohl, Phys. Rev. X **7**, 031007 (2017).
[28] C. Carr, R. Ritter, C. G. Wade, C. S. Adams, and K. J. Weatherill, Phys. Rev. Lett. **111**, 113901 (2013).
[29] T. Baluktsian, B. Huber, R. Löw, and T. Pfau, Phys. Rev. Lett. **110**, 123001 (2013).
[30] A. Urvoy, F. Ripka, I. Lesanovsky, D. Booth, J. P. Shaffer, T. Pfau, and R. Löw, Phys. Rev. Lett. **114**, 203002 (2015).
[31] L. Zhang and J. Evers, Phys. Rev. A **94**, 033402 (2016).
[32] F. Ripka, H. Kübler, R. Löw, and T. Pfau, Science **362**, 446 (2018).
[33] S. Briaudeau, S. Saltiel, G. Nienhuis, D. Bloch, and M. Ducloy, Phys. Rev. A **57**, R3169 (1998).

[34] M. Fichet, G. Dutier, A. Yarovitsky, P. Todorov, I. Hamdi, I. Maurin, S. Saltiel, D. Sarkisyan, M.-P. Gorza, D. Bloch, and M. Ducloy, Europhys. Lett. **77**, 54001 (2007).
[35] D. Sarkisyan, T. Varzhapetyan, A. Sarkisyan, Y. Malakyan, A. Papoyan, A. Lezama, D. Bloch, and M. Ducloy, Phys. Rev. A **69**, 065802 (2004).
[36] S. A. Moiseev and S. Kröll, Phys. Rev. Lett. **87**, 173601 (2001).
[37] S. L. McCall and E. L. Hahn, Phys. Rev. Lett. **18**, 908 (1967).
[38] A. Omont, J. Phys. II (France) **38**, 1343 (1977).
[39] I. L. Beigman and V. S. Lebedev, Phys. Rep. **250**, 95 (1995).
[40] Energy dependence of the electron-atom scattering is neglected as the average velocity of a Rydberg electron $\sim v_0/n$ is far larger than the typical velocity of atoms at room temperature.
[41] See Supplemental Material at http://link.aps.org/supplemental/10.1103/PhysRevLett.125.263605 for additional details about the model, mean field calculation, cross-phase modulation, and simulatons, which includes Refs. [10,11,39,42–48].
[42] D. Tong, S. M. Farooqi, J. Stanojevic, S. Krishnan, Y. P. Zhang, R. Côté, E. E. Eyler, and P. L. Gould, Phys. Rev. Lett. **93**, 063001 (2004).
[43] O. Firstenberg, M. Shuker, R. Pugatch, D. R. Fredkin, N. Davidson, and A. Ron, Phys. Rev. A **77**, 043830 (2008).
[44] V. Lebedev and V. Marchenko, J. Exp. Theor. **88**, 754 (1985), http://www.jetp.ac.ru/cgi-bin/e/index/e/61/3/p443?a=list.
[45] D. A. Steck, Alkali D Line Data (2019), https://steck.us/alkalidata/.
[46] T. Pohl, E. Demler, and M. D. Lukin, Phys. Rev. Lett. **104**, 043002 (2010).
[47] D. Paredes-Barato and C. S. Adams, Phys. Rev. Lett. **112**, 040501 (2014).
[48] J. P. Boyd, *Chebyshev and Fourier Spectral Methods: Second Revised Edition*, 2nd ed. (Dover Publications, New York, 2001).
[49] A. M. Hankin, Y.-Y. Jau, L. P. Parazzoli, C. W. Chou, D. J. Armstrong, A. J. Landahl, and G. W. Biedermann, Phys. Rev. A **89**, 033416 (2014).
[50] Y.-Y. Jau, A. M. Hankin, T. Keating, I. H. Deutsch, and G. W. Biedermann, Nat. Phys. **12**, 71 (2016).
[51] J. Wang, J. Bai, J. He, and J. Wang, Opt. Express **25**, 22510 (2017).
[52] B. Li, M. Li, X. Jiang, J. Qian, X. Li, L. Liu, and Y. Wang, Phys. Rev. A **99**, 042502 (2019).
[53] C. H. Greene, A. S. Dickinson, and H. R. Sadeghpour, Phys. Rev. Lett. **85**, 2458 (2000).
[54] V. Bendkowsky, B. Butscher, J. Nipper, J. P. Shaffer, R. Löw, and T. Pfau, Nature (London) **458**, 1005 (2009).
[55] W. Li, T. Pohl, J. M. Rost, S. T. Rittenhouse, H. R. Sadeghpour, J. Nipper, B. Butscher, J. B. Balewski, V. Bendkowsky, R. Löw, and T. Pfau, Science **334**, 1110 (2011).
[56] J. P. Shaffer, S. T. Rittenhouse, and H. R. Sadeghpour, Nat. Commun. **9**, 1965 (2018).
[57] F. Camargo, R. Schmidt, J. D. Whalen, R. Ding, G. Woehl, S. Yoshida, J. Burgdörfer, F. B. Dunning, H. R. Sadeghpour, E. Demler, and T. C. Killian, Phys. Rev. Lett. **120**, 083401 (2018).
[58] A. Urvoy, C. Carr, R. Ritter, C. S. Adams, K. J. Weatherill, and R. Löw, J. Phys. B **46**, 245001 (2013).
[59] G. L. Lamb, Rev. Mod. Phys. **43**, 99 (1971).
[60] N. Šibalić, J. M. Kondo, C. S. Adams, and K. J. Weatherill, Phys. Rev. A **94**, 033840 (2016).
[61] T. P. Ogden, K. A. Whittaker, J. Keaveney, S. A. Wrathmall, C. S. Adams, and R. M. Potvliege, Phys. Rev. Lett. **123**, 243604 (2019).
[62] P. G. P. Agrawal, *Nonlinear Fiber Optics* (Academic Press, New York, 2012).
[63] M. N. Islam, Opt. Lett. **14**, 1257 (1989).
[64] R. McLeod, K. Wagner, and S. Blair, Phys. Rev. A **52**, 3254 (1995).
[65] B. A. Kochetov, I. Vasylieva, A. Butrym, and V. R. Tuz, Phys. Rev. E **99**, 052214 (2019).